Electronic Supplementary Material (ESI) for Physical Chemistry Chemical Physics.
This journal is © the Owner Societies 2022

Supporting Information

A new ratiometric switch "two-way" detects hydrazine and hypochlorite via "dye-release" mechanism with PBMCs bioimaging study

Sangita Das, [a, b, c*] Lakshman Patra, [a] Partha Pratim Das, [d] Kakali Ghoshal, [e] Saswati Gharami, [a] James. W. Walton, [b] Maitree Bhattacharyya [e] and Tapan Kumar Mondal [a, *]

[a.] *Department of Chemistry, Jadavpur University, Kolkata -700032, India.*

[b.] *Durham University, Department of Chemistry. Durham, DH1 3LE, UK, Email: sangita.das@durham.ac.uk; sangitadas2327@gmail.com, sangita.das@kist-europe.de*

[c.] *KIST Europe Forschungsgesellschaft mbH, Campus E71, 66123 Saarbrücken, Germany*

[d.] *Center for Novel States of Complex Materials Research, Seoul National University, Seoul 08826, Republic of Korea*

[e.] *Department of Biochemistry, University of Calcutta, Kolkata-700019, India*

CONTENTS

1. ***Experimental*……..**
2. **X-ray crystallography…….**
3. ***Selectivity study*……..**
4. ***Determination of detection limit*……...**
5. ***Linear responsive curves of the probes depending on N_2H_4 and OCl^- concentration*….....**
6. ***Determination of Quantum yield*……..**
7. ***pH study*……..**
8. ***Time dependent fluorescence spectra of HQCN with added N_2H_4*.....**
9. ***Time dependent fluorescence spectra of HQCN with added OCl^-*.....**
10. ***Computational study*……..**
11. ***Bioimaging and MTT assay* ……..**

12. ^{1}H NMR spectrum of HQCN ……....

13. ^{13} C NMR spectrum of HQCN ……..…..

14. Mass spectrum (HRMS) of HQCN ……...

15. MS spectrum of the product (HQCN with N_2H_4)……...

16. MS spectrum of the product (HQCN with OCl^-)……...

17. Comparison Table…….

18. References……...

1. Experimental

General

Unless otherwise mentioned, materials were obtained from commercial suppliers and were used without further purification. Thin layer chromatography (TLC) was carried out using Merck 60 F_{254} plates with a thickness of 0.25 mm. ^{1}H and ^{13}C NMR spectra were recorded on Brucker 300 MHz instruments. For NMR spectra, $CDCl_3$ was used as solvent using TMS as an internal standard. Chemical shifts are expressed in δ units and ^{1}H–^{1}H and ^{1}H–C coupling constants in Hz. UV-vis spectra were recorded on a PerkinElmer lambda 750 spectrometer. Fluorescence spectra were recorded on Shimadzu RF-6000 fluorescence spectrometer. For the titration experiment we used the anions, amines and different neutral analytes viz. [different guest analytes such as hydroxylamine, ammonia, ethylenediamine, hydrazine, methylamine, n-butylamine, ethylenediamine, ammonia, thiourea, triethylamine H_2O_2, S^{2-}, N_3^-, NO_2^-, NO_3^-, I^-, Cl^-, F^-, SO_4^{2-}, $OONO^-$, O^{2-}, ^{t}-BuOOH] anions as their sodium salts.

General method of UV-Vis absorption and fluorescence emission titrations:

For both UV-Vis and fluorescence titrations, a stock solution of **HQCN** was prepared (10 μM) in CH_3OH-H_2O (1/4, v/v) in the presence of HEPES buffer (10 mM) solution at pH = 7.2. The solution of the guest anions using their sodium salts at 10 μM were prepared in buffered deionised water at pH 7.2. The absorption spectra of these solutions were recorded by means of UV-Vis methods using a 10 mm path length quartz cuvette. Fluorescence emission was measured in a 10 mm path length quartz cuvette with the excitation wavelength 370 nm. Fluorescence lifetimes were measured using a time-resolved spectrofluorometer from IBH, UK. The instrument uses a picoseconds diode laser (NanoLed-07, 370 nm) as the excitation source and works on the principle of time-correlated single photon counting. The goodness of fit was evaluated by χ^2 criterion and visual inspection of the residuals of the fitted function to the data.

Materials and methods
Details of bio-imaging

Venous blood (3ml) was obtained by venepuncture from a healthy male volunteer donor (age - 30 years) with informed consent. The research program was approved by Calcutta University Biosafety and Ethics Committee. Peripheral blood mononuclear cells were isolated with histopaque-1077 gradient [SIGMA] through density gradient centrifugation. PBMCs were washed in ice cold PBS for two times and resuspended in the same with a cell density of 3 X 10^6. PBMCs were treated with or without N_2H_4 (25 μM) and **HQCN** (10 μM) and incubated for 30 minutes at 37 ^{0}C in dark. **HQCN** samples were prepared in DMSO and PBS (1:1). The fluorescence intensity was measured in fluorescence microscope (Carl Zeiss HBO 100) under 40X magnification with fluorescence emissions

at 620 nm (Red channel, Filter set 42) nm and 450 nm (Blue channel, Filter Set 9) respectively. The relative fluorescence intensities were quantitated using ImageJ software.

6 ml of venous blood was obtained from from a healthy male volunteer donor (age - 30 years) with informed consent maintaining ethical guidelines of Calcutta University. Peripheral blood mononuclear cells or PBMCs (lymphocytes and monocytes) were isolated within one hour of sampling by density gradient centrifugation using histopaque-1077 (Sigma) by centrifuging at 400×g for 30–40 min at room temperature. The middle layer or 'buffy coats' contains the PBMCs which were collected, washed and allowed to grow in supplemented DMEM in cell culture plate for 3 hour in a humidified 37°C, 5% CO_2 incubator. Adherent monocytes were scraped gently from the plate bottom and suspended in HBSS (pH 7.4). Observed cell viability was ~90% as checked by Trypan Blue exclusion and cell count noted to be 1×10^6 in 500 µl of cell suspension. HQCN samples were prepared in 50% DMSO and 50% PBS. Monocytes were then incubated with 10 µM HQCN sample for 50 minutes at 37^0 C. Cells were observed under fluorescence microscope (Carl Zeiss HBO 100) with fluorescence emissions at 620 and 500 nm respectively.

MTT assay

To determine cell viability against HQCN, PBMCs were treated with different concentrations of HQCN solution (upto 50 µM) for 1 hour at 37°C against control cell suspension with no added HQCN. Cell density remains 10^6 cells per well in a 96- well plate. 100 µl of MTT solution (5mg/ml) was added to each well including control and incubated for 4 hours at 37°C. The purple coloured formazan crystals were dissolved in 100 µl DMSO and the absorbance were measured at 570 nm. Cell viability was calculated using the following calculation:

$$\% \text{ of Cell Viability} = \frac{(\text{Absorbance of treatment group - blank})}{(\text{Absorbance of control group - blank})} \text{ X } 100$$

2. X-ray crystallography

Single crystals were obtained by slow evaporation of methanolic solution of HQCN. X-ray data were collected using an automated Bruker AXS Kappa smart Apex-II diffractometer equipped with an Apex-II CCD area detector using a fine focus sealed tube as the radiation source of graphite monochromated Mo Kα radiation (λ = 0.71073 Å). Details of crystal analyses, data collection and structure refinement are summarized in Table S1. Reflection data were recorded using the ω scan technique. The structure was solved and refined by full-matrix least-squares techniques on F^2 using the SHELXL-2016/6. [1] The absorption corrections were done by multi-scan (SHELXTL program

package) and all the data were corrected for Lorentz, polarization effect. Hydrogen atoms were included in the refinement process as per the riding model. The crystallographic data have been deposited to the Cambridge Crystallographic Data Center: Deposition numbers CCDC 1858041.

Single crystals of the sensor (HQCN) suitable for X-ray studies were obtained by dissolving powder of the pure compound in $CHCl_3$: CH_3CN (1: 9, v/v) and slow evaporation of the solution. A summary of the crystallographic data is given in Table S1.

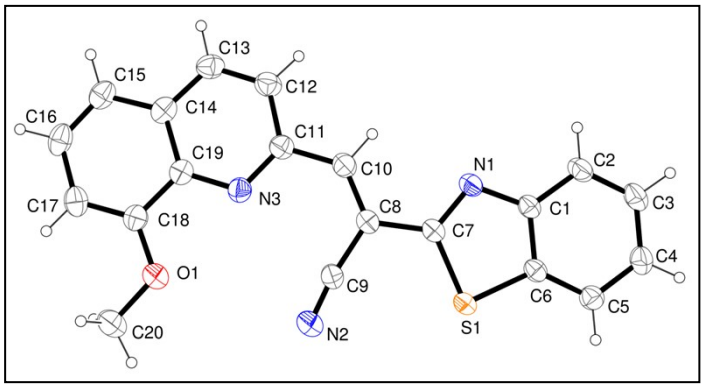

Figure S1: ORTEP of **HQCN** with 35% ellipsoidal probability (selected bond distances (Å): O1-C18, 1.354(2); S1-6, 1.7282(17); S1-C7, 1.7453(18); N1-C1, 1.381(2); N1-C7, 1.300(2); N2-C9, 1.143(2); N3-C11, 1.327(2); N3-C19, 1.357(2); C8-C10, 1.345(2) and C8-C9, 1.435(2)

Table S1: Crystallographic data and refinement parameters of H_2L.

Formula	$C_{20}H_{13}N_3O\,S$
Formula Weight	343.39
Crystal System	*Monoclinic*
Space group	*P21/n*
a, b, c [Å]	15.8363(12), 5.1256(4), 20.6360(16)
β [°]	103.118(3)
V [$Å^3$]	1631.3(2)
Z	4
D(calc) [g/cm^3]	1.398
μ (Mo Kα) [mm^{-1}]	0.211
F(000)	712
Absorption Correction	*multi-scan*
Temperature (K)	293(2)
Radiation [Å]	0.71073
θ(Min-Max) [º]	1.838- 27.158
Dataset (h; k; l)	-20 and 20; -6 and 6; -26 and 26

Total, Unique Data, R(int)	52254/3605/0.0671
Observed data [I > 2σ(I)]	2727
Nref, Npar	3605/226
R, wR_2	0.0391, 0.0977
Δq(max) and Δq(min) [e/Å^3]	0.165 and -0.199
Goodness of fit(S)	1.038

3. Selectivity study

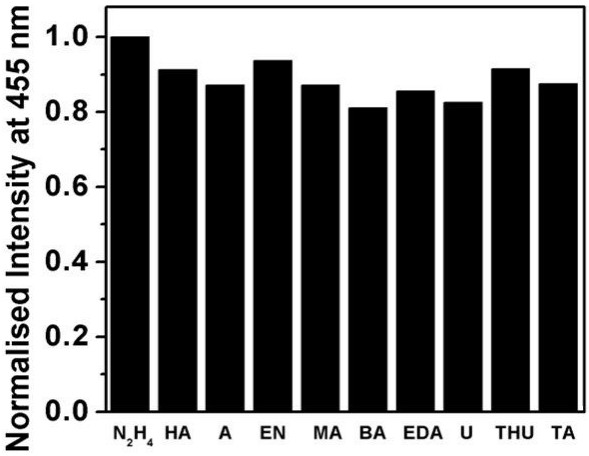

Figure S2: A comparative study of emission intensity of HQCN at 455 nm after addition of different analytes (3 equivalents) in the solution of HQCN (10 μM) in presence of N_2H_4 (2 equivalents), (The different analytes are, HA=hydroxylamine, A = ammonia, EN = ethylamine, MA = methylamine, BA = n-butylamine, EDA = ethylene diamine, THU = Thiourea, TA = Triethylamine. λ_{ex} = 370 nm.)

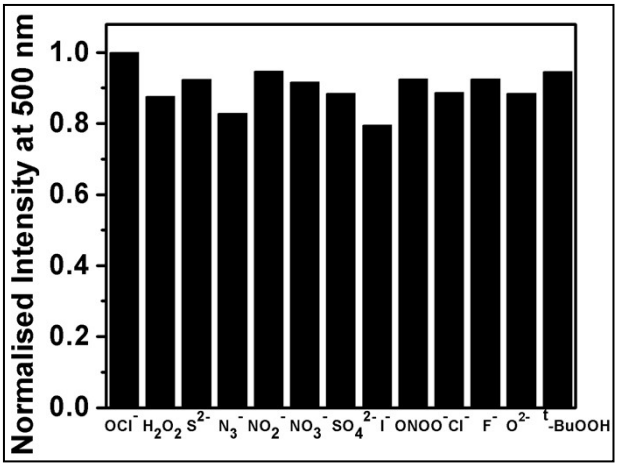

Figure S3: A comparative study of emission intensity of HQCN at 500 nm after addition of different analytes (3 equivalents) in the solution of HQCN (10 μM) in presence of OCl^- (2 equivalents) λ_{ex} = 370 nm.

4. **Determination of detection limit:** (For N_2H_4)

The detection limit was calculated based on the fluorescence titration. To determine the S/N ratio, the emission intensity of **HQCN** without N_2H_4 was measured by 10 times and the standard deviation of blank measurements was determined. The detection limit (DL) of **HQCN** for N_2H_4 was determined from the following equation: DL = K × Sb_1/S, where K = 2 or 3 (we take 3 in this case); Sb_1 is the standard deviation of the blank solution; S is the slope of the calibration curve. For N_2H_4:

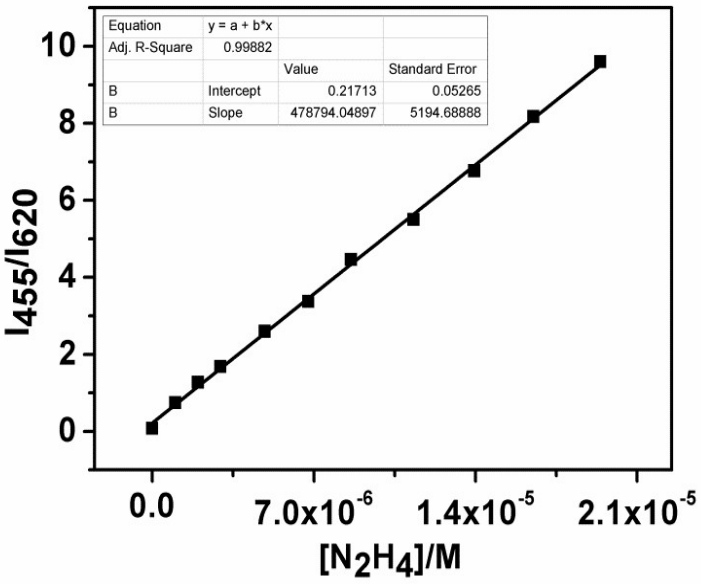

Figure S4: Emission intensity ratio I_{455}/I_{620} of HQCN depending on the concentration of N_2H_4

From the graph we get slope = 478794.048, and Sb_1 value is 0.00360
Thus using the formula we get the Detection Limit = 2.25 × 10^{-8} M i.e. HQCN can detect N_2H_4 in this minimum concentration through fluorescence method.

Determination of detection limit: (For OCl^-)

The detection limit was calculated based on the fluorescence titration. To determine the S/N ratio, the emission intensity of **HQCN** without OCl^- was measured by 10 times and the standard deviation of blank measurements was determined.

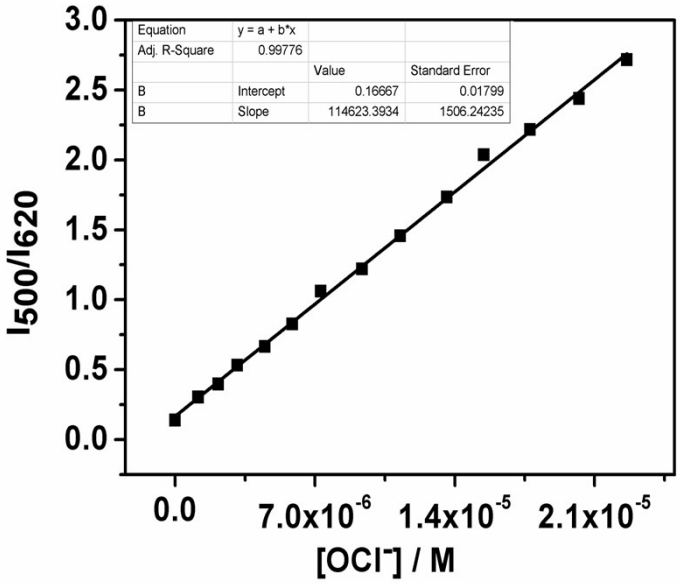

Figure S5: Emission intensity ratio (I_{500}/I_{620}) of HQCN depending on the concentration of OCl^-

The detection limit (DL) of **HQCN** for N_2H_4 was determined from the following equation: DL = K × Sb_1/S, where K = 2 or 3 (we take 3 in this case); Sb_1 is the standard deviation of the blank solution; S is the slope of the calibration curve. For N_2H_4:

From the graph we get slope =114623.3934, and Sb_1 value is 0.0013231

Thus using the formula, we get the Detection Limit = 3.46 × 10^{-8} M i.e. HQCN can detect N_2H_4 in this minimum concentration through fluorescence method.

5. Linear responsive curve of HQCN depending on N_2H_4 concentration:

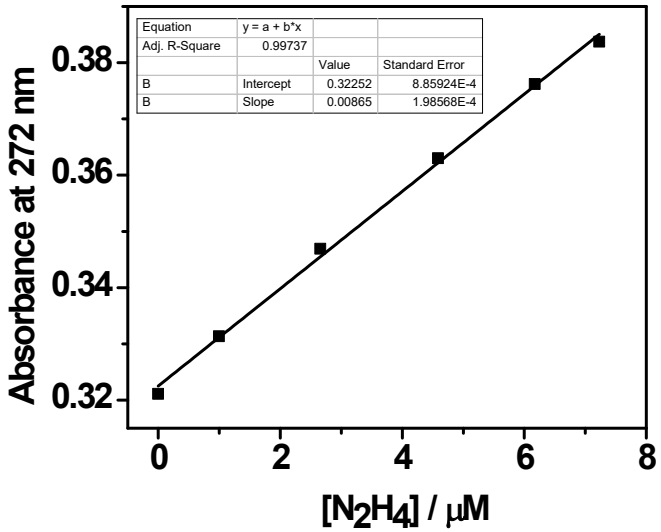

Figure S6: The linear responsive curve with absorbance at 272 nm of **HQCN** depending on the N_2H_4 concentration.

Linear responsive curve of HQCN depending on OCl^- concentration:

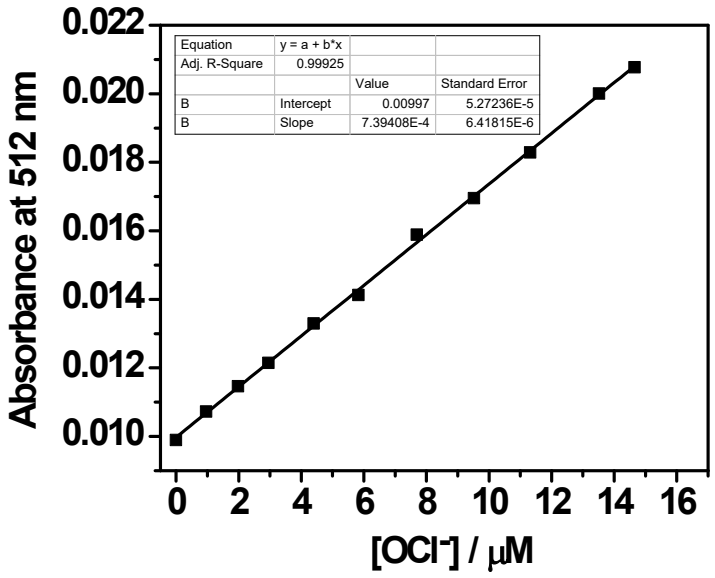

Figure S7: The response curve of HQCN absorbance at 512 nm depending on the OCl^- concentration.

6. **Determination of fluorescence Quantum Yields (Φ) of HQCN and its complex with N_2H_4 and OCl^- :**

For measurement of the quantum yields of HQCN and its complex with N_2H_4, we recorded the absorbance of the compounds in methanol solution. The emission spectra were recorded using the maximal excitation wavelengths, and the integrated areas of the fluorescence-corrected spectra were measured. The quantum yields were then calculated by comparison comparison with fluorescein (Φs = 0.97 in basic ethanol) as reference using the following equation:

$$\Phi x = \Phi s \times \left(\frac{Ix}{Is}\right) \times \left(\frac{As}{Ax}\right) \times \left(\frac{nx}{ns}\right)^2$$

Where, x & s indicate the unknown and standard solution respectively, Φ is the quantum yield, *I* is the integrated area under the fluorescence spectra, *A* is the absorbance and *n* is the refractive index of the solvent.

We calculated the quantum yield of HQCN, HQCN- N_2H_4 and HQCN-OCl^- using the above equation and the value is 0.39, 0.24 and 0.45 respectively.

7. pH dependent study:

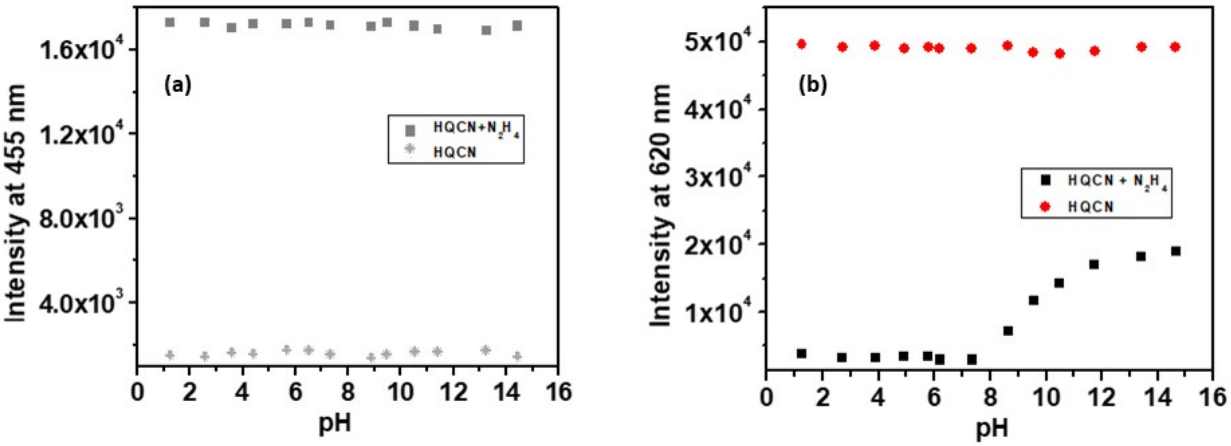

Figure S8: Fluorescence response of only HQCN and HQCN + $\mathbf{N_2H_4}$ at (a) 455 nm and (b) 620 nm as a function of pH in MeOH/ H_2O (1/ 1, *v/v*), pH is adjusted by using aqueous solutions of 1 M HCl or 1 M NaOH. [HQCN] = 10 μM, [N_2H_4] = 60 μM. λ_{ex} = 370 nm.

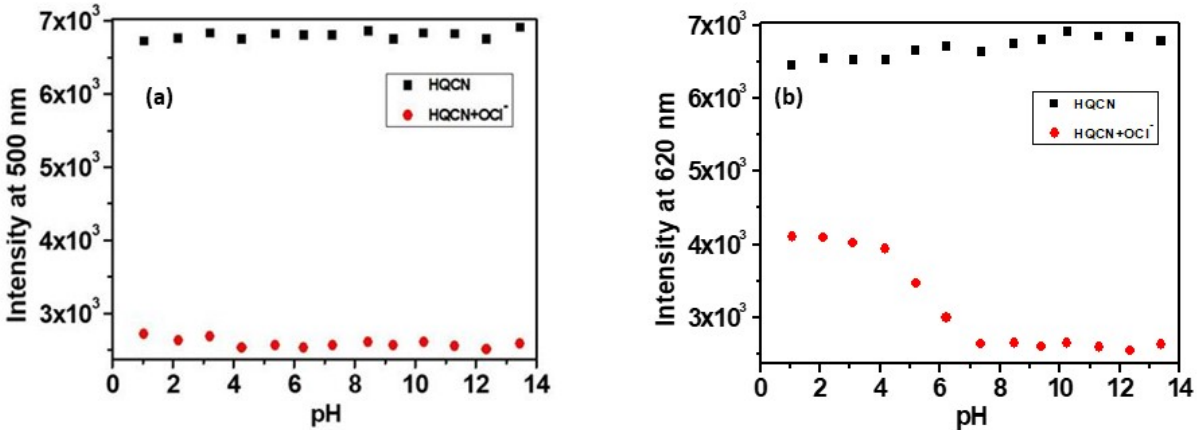

Figure S9: Fluorescence response of only HQCN and HQCN + $\mathbf{OCl^-}$ at (a) 500 nm and (b) 620 nm as a function of pH in MeOH/ H_2O (1/ 1, *v/v*), pH is adjusted by using aqueous solutions of 1 M HCl or 1 M NaOH. [HQCN] = 10 μM, [OCl^-] = 60 μM. λ_{ex} = 370 nm.

8. Time dependent fluorescence spectra of HQCN with added N_2H_4

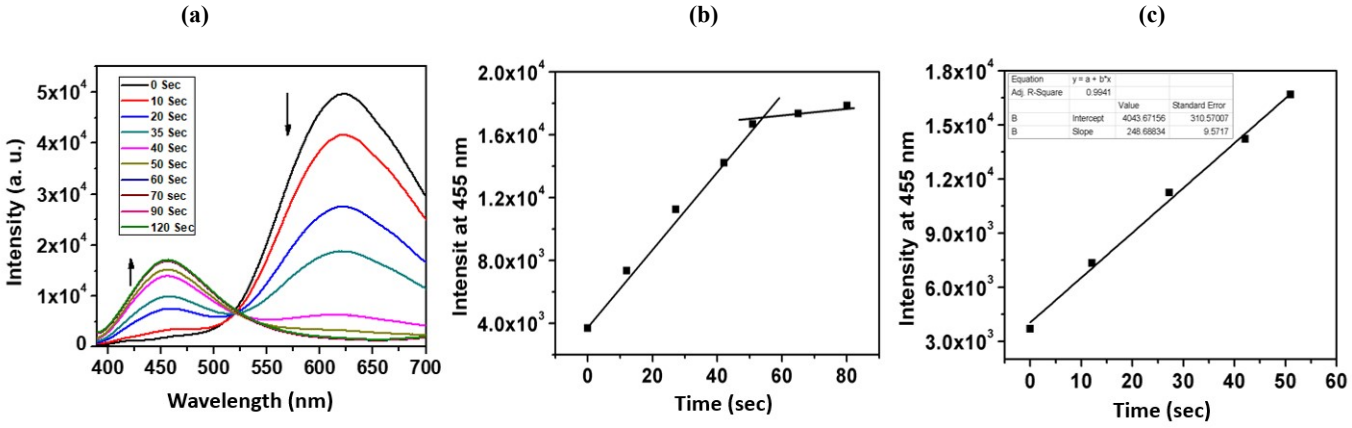

Figure S10: (a) Change of emission spectra of HQCN (10 μM) upon addition of hydrazine (2 equivalents), (b) Time dependent fluorescence spectra of HQCN at 455 nm after interaction hydrazine with time. (c) Linear relationship of emission of HQCN at 455 nm after interaction hydrazine with time.

9. Time dependent fluorescence spectra of HQCN with added OCl^-

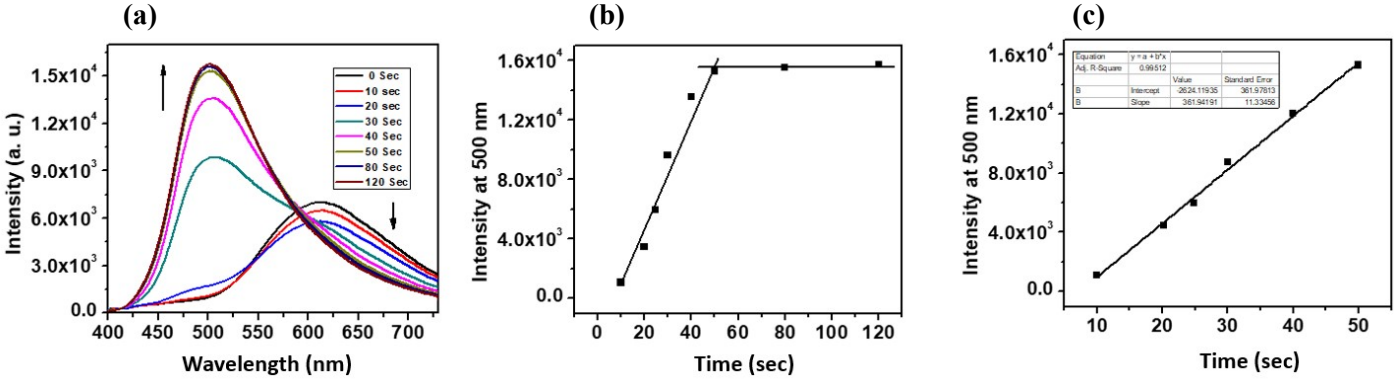

Figure S11: (a) Change of emission spectra of HQCN (10 μM) upon addition of OCl^- (2 equivalents), (b) Time dependent fluorescence spectra of HQCN at 500 nm after interaction OCl^- with time. (c) Linear relationship of emission of HQCN at 500 nm after interaction OCl^- with time.

Table S2: Fluorescence life-time data of HQCN

Entry	Φ	τ (ns)	k_r ($10^8 \times s^{-1}$)	k_{nr} ($10^8 \times s^{-1}$)
HQCN	0.39	0.7	5.56	8.7
HQCN-N_2H_4	0.24	6.32	0.37	1.13
HQCN-OCl^-	0.45	5.75	0.78	0.92

10. **Computational study:**

Full geometry optimizations were carried out using the density functional theory (DFT) method at the B3LYP/6-31+G(d) [2-4] level for the compounds. The vibrational frequency calculations were performed to ensure that the optimized geometries represent the local minima and there were only positive eigen values. Vertical electronic excitations based on B3LYP optimized geometries were computed using the time-dependent density functional theory (TDDFT) formalism [5-7] in methanol using conductor-like polarizable continuum model (CPCM) [8-10]. All calculations were performed with Gaussian09 program package [11] with the aid of the GaussView visualization program.

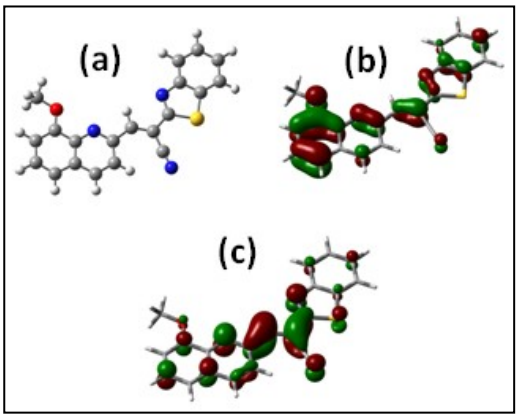

Figure S12: Optimized structures, HOMO and LUMO orbitals of HQCN calculated at the DFT level using the B3LYP/6-311G+(d,p) basis set.

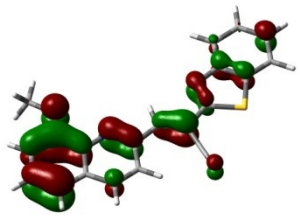	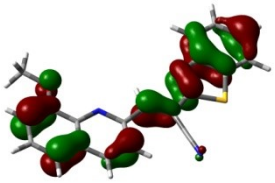	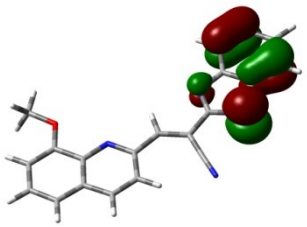
HOMO E = -5.84 eV	HOMO-1 E = -6.28 eV	HOMO-2 E = -6.48 eV
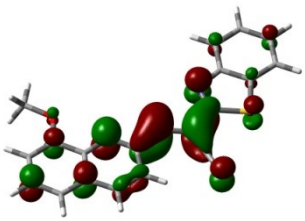	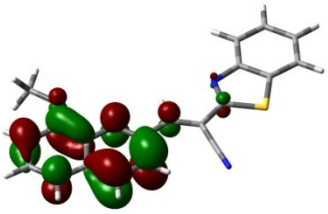	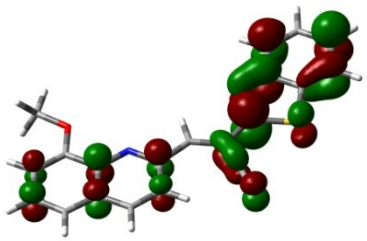
LUMO E= -2.61 eV	LUMO+1 E= -1.26 eV	LUMO+2 E = -0.66 eV

Figure S13: Contour plot of selected molecular orbitals of **HQCN**

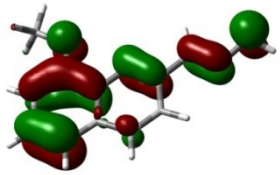	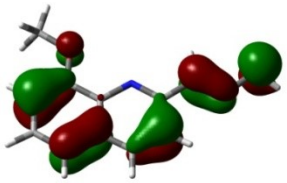	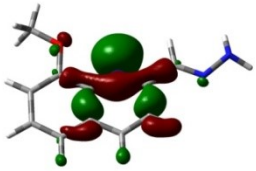
HOMO E = -5.42 ev	HOMO-1 E = -5.97 ev	HOMO-2 E = -6.68 ev
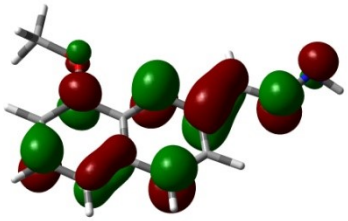	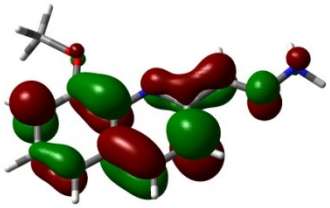	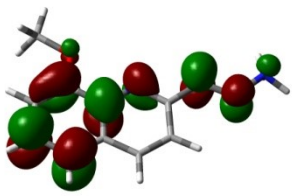
LUMO E = -1.28 ev	LUMO+1 E = -0.62 ev	LUMO+2 E = 0.76 ev

Figure S14: Contour plot of selected molecular orbitals of **HQCN-N_2H_4 complex.**

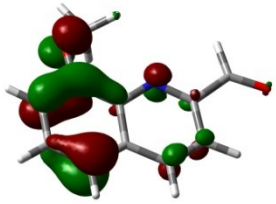	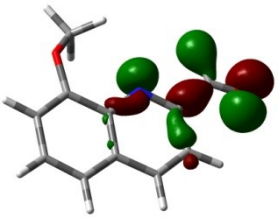	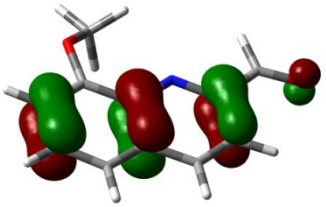
HOMO E = - 5.99 ev	HOMO-1 E = -6.94 ev	HOMO-2 E = -7.13 ev
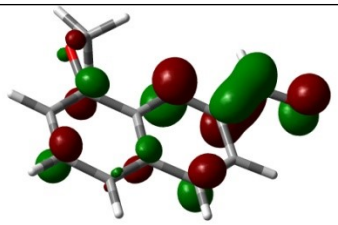	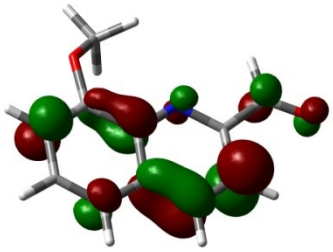	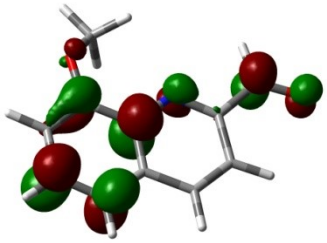
LUMO E = -2.18 ev	LUMO+1 E = -1.22 ev	LUMO+2 E = 0.20 ev

Figure S15: Contour plot of selected molecular orbitals of **HQCN-OCl$^-$ (HQA) complex.**

Compound	Excitation	Excitation wavelength (nm)	Oscillator strength (au)	Energy (eV)
HQCN	HOMO→LUMO (95%) HOMO-1→LUMO (94%) HOMO-2→LUMO (98%) HOMO→LUMO +1(67%)	461.47 392.12 373.11 302.74	0.4150 0.6966 0.0873 0.2740	2.6867 3.1619 3.3230 4.0954
HQCN-N_2H_4	HOMO→ LUMO (84%) HOMO→ LUMO+1(46%) HOMO-1→ LUMO+1(85%)	336.11 277.93 256.76	0.2183 0.9427 0.0281	3.6888 4.4610 4.8287
HQCN-OCl$^-$	HOMO→LUMO (92 %) HOMO-2→LUMO (72%)	379.03 253.42	0.0567 0.5423	3.2711 4.8925

Table S3: Vertical electronic excitations of **HQCN, HQCN-N_2H_4** and HQCN-OCl$^-$ **(HQA)** calculated by TDDFT/B3LYP/CPCM method.

11. Bioimaging and MTT assay

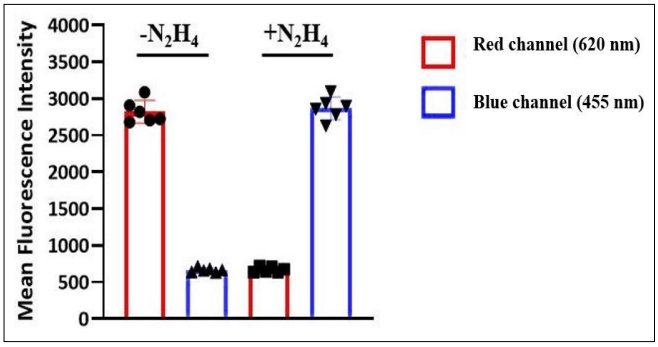

Figure S16: The mean fluorescence intensities were measured in ImageJ, which shows a significant ($P < 0.05$) shifts from red channel to blue channel fluorescence when hydrazine was added. When there was no hydrazine present red fluorescence was significantly ($P < 0.05$) more visible than blue. The P values were calculated using one-way ANOVA followed by multiple comparison for differences between groups.

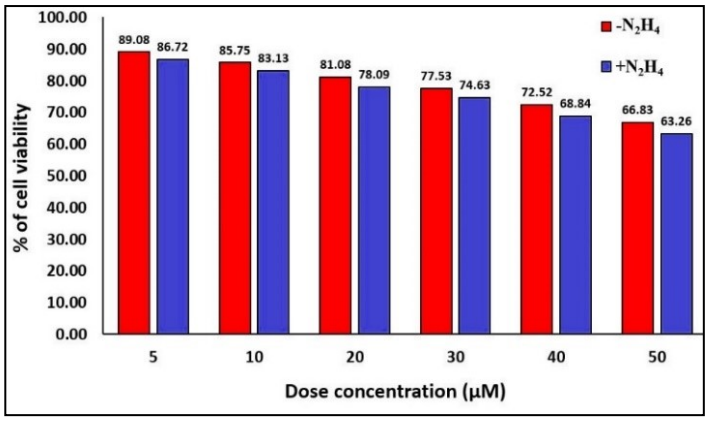

Figure S17: Percentage of viable cells over HQCN concentration range (5-50 µM) presence and absence of N_2H_4.

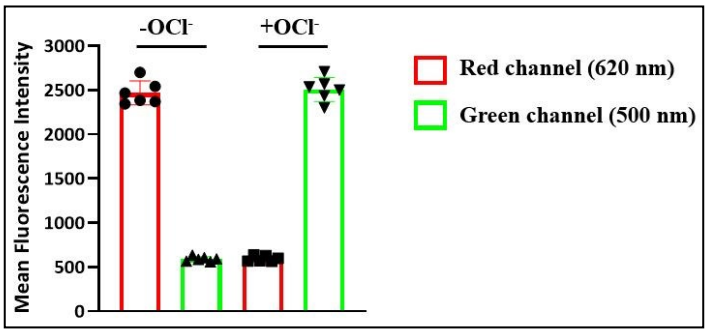

Figure S18: The mean fluorescence intensities were measured in Image, which shows a significant ($P < 0.05$) shifts from red (577 ± 39.8) to green (2795 ± 156.8) fluorescence when OCl- was added. When there was no OCl- present red fluorescence (2362.3 ± 224.1) was significantly ($P < 0.05$) more visible than green (552.6 ± 45.2). The P values were calculated using one-way ANOVA followed by multiple comparison for differences between groups.

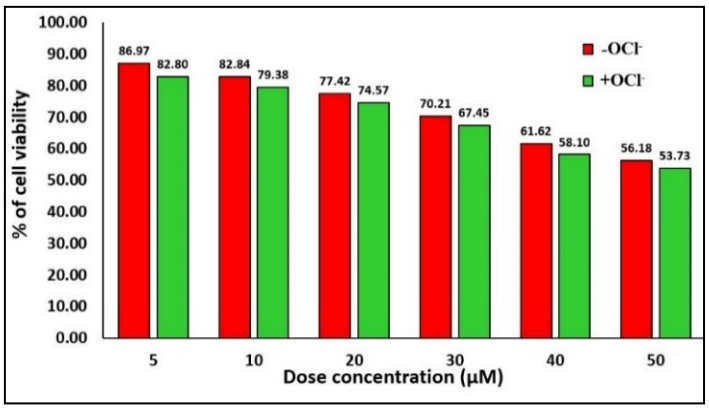

Figure S19: Percentage of viable cells over HQCN concentration range (5-50 µM) presence and absence of OCl^-.

12. [1]H NMR spectrum of HQCN

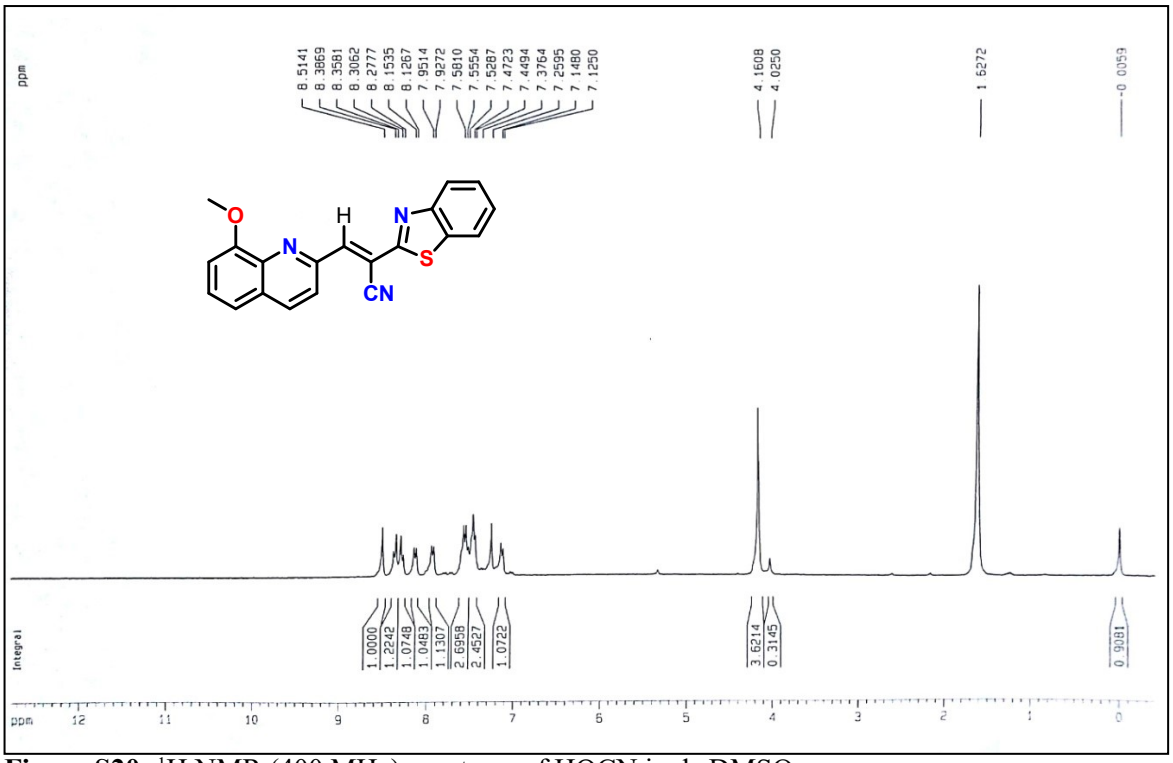

Figure S20: [1]H NMR (400 MHz) spectrum of HQCN in d_6-DMSO

13. [13]C NMR spectrum of HQCN

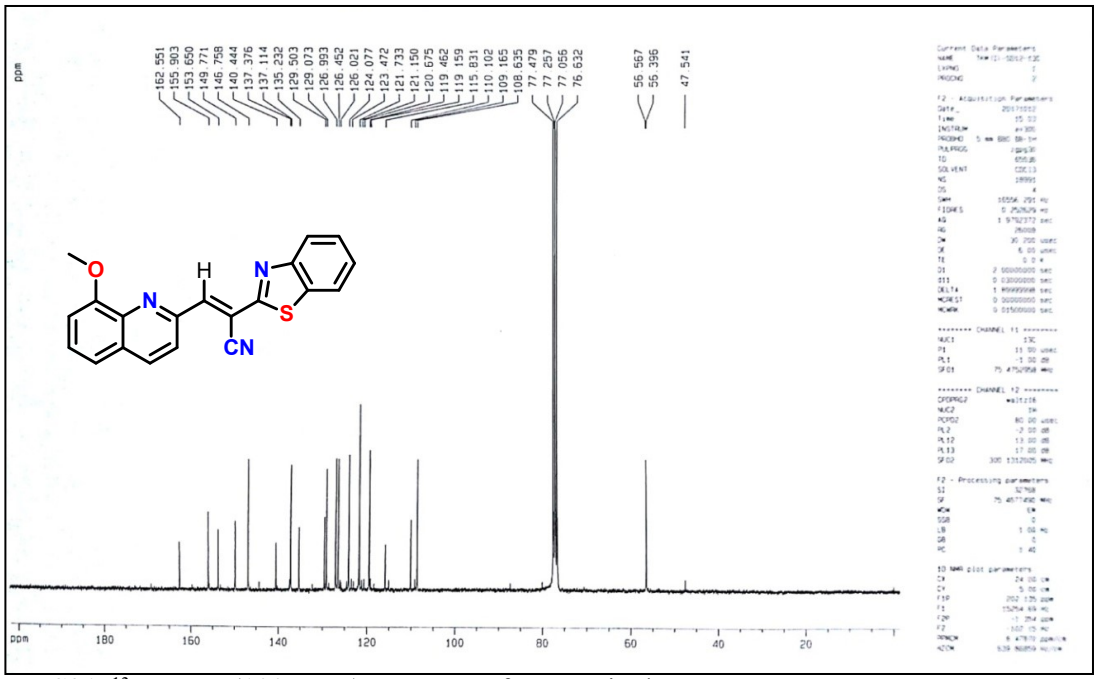

Figure S21: [13]C NMR (100 MHz) spectrum of HQCN in d_6-DMSO

14. Mass spectrum (HRMS) of HQCN

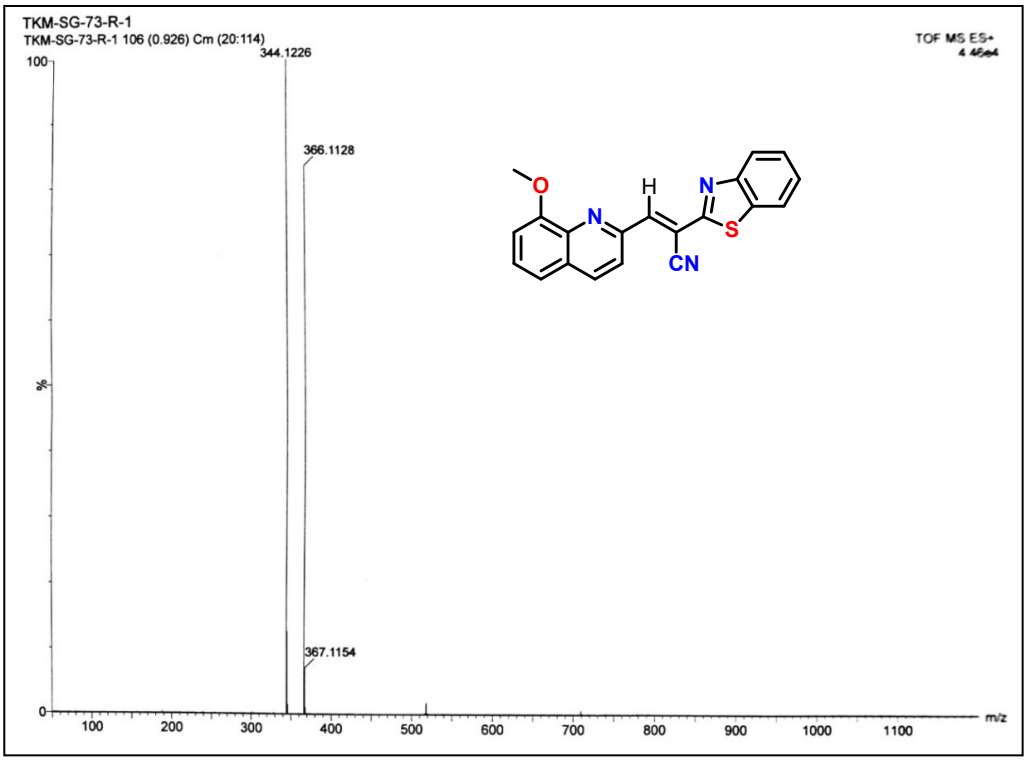

Figure S22: HRMS of HQCN.

15. MS spectrum of the product (HQCN with N_2H_4)

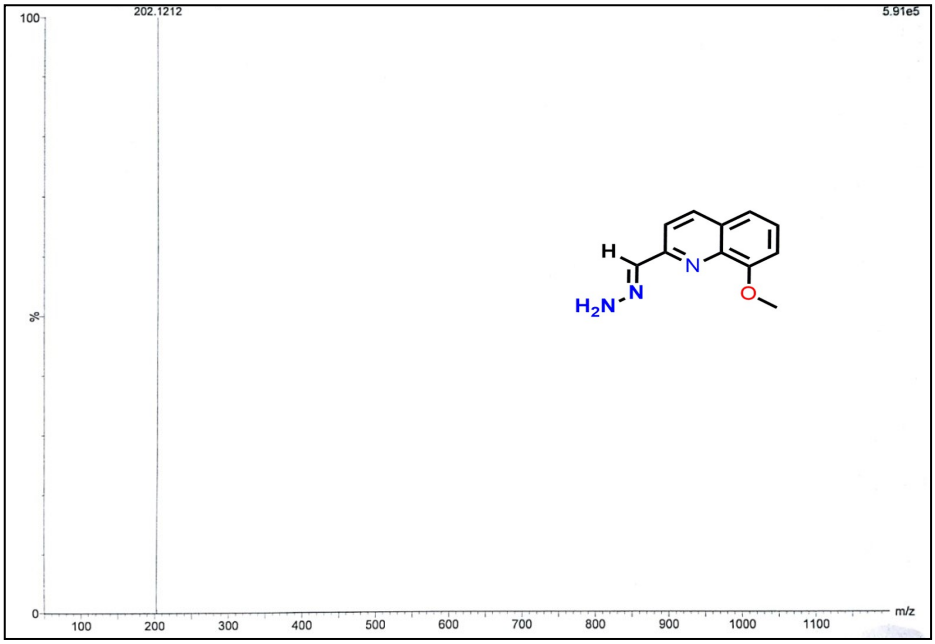

Figure S23: HRMS of HQCN+N_2H_4 Complex.

16. MS spectrum of the product (HQCN with OCl^-)

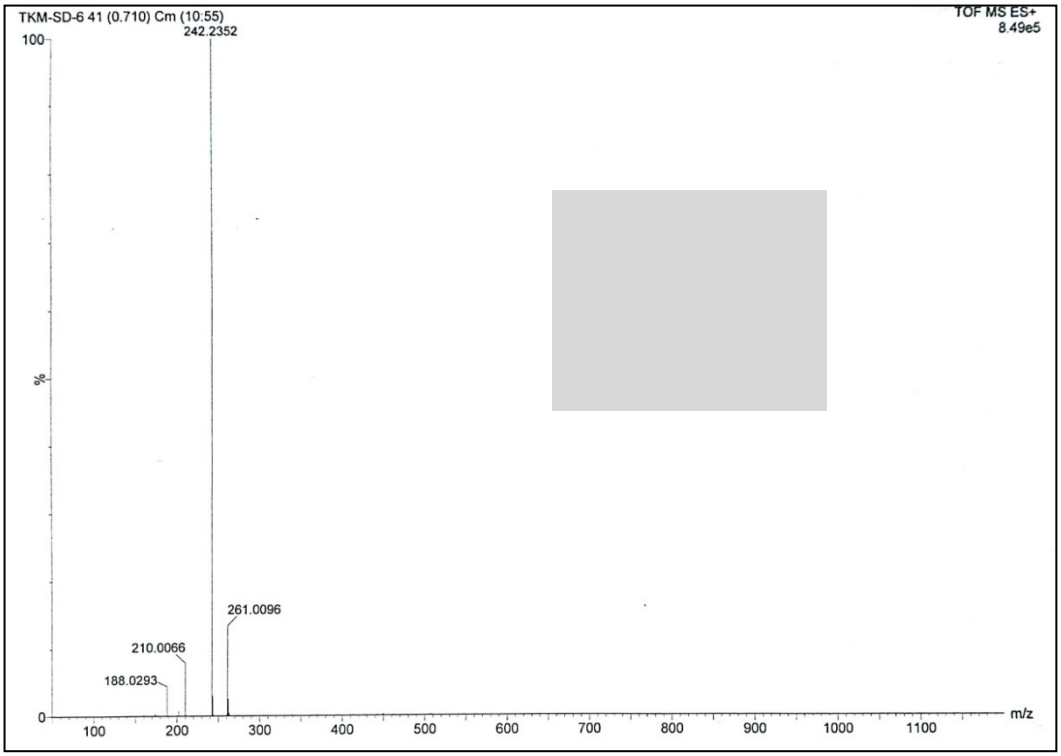

Figure S24: HRMS of HQCN+OCl^- complex.

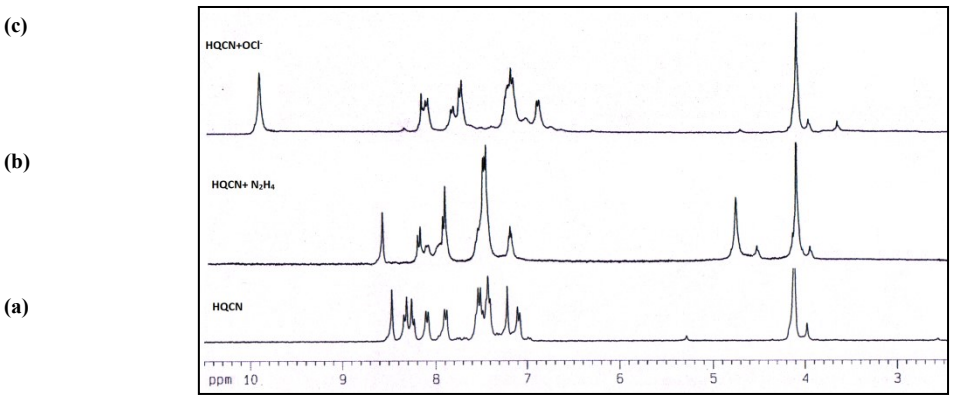

Figure S25: ^1H NMR (400 MHz) spectra of (a) HQCN (Conc. = 7.2×10^{-3} M), (b) [HQCN+ N_2H_4] (3.6×10^{-3} M)], (c) [HQCN + OCl^-] (Conc. = 7.2×10^{-3} M) in d^6 DMSO containing 1% D_2O.

17. Comparison Table

Table S4

Sr. No	**Fluorophore Used**	**Ratiometric Fluorescence Change** (Detection method)	**Detection Limit**	**Bioimaging Studies (N_2H_4 and OCl^- detection)**	**Bioimaging Studies With** Human **PBMCs**	**References**	**Sensing Guest Analytes**
1.	Xanthen-2H-indene-1,3-dione	No	75 nM	Only N_2H_4	No	New J. Chem., 2021, 45, 15869–15875.	N_2H_4
2.	Carbazole-naphthalimide	No	65 nM	Only N_2H_4	No	New J. Chem., 2021, 45, 17095–17100.	N_2H_4
3.	Carbazol-indene-dione	No	4.94 x 10^{-7} mol L^{-1}	Only N_2H_4	No	New J. Chem., 2021, 45, 21151–21159 |	N_2H_4
4.	Styryl bridge containing a triphenylamine–thioimidazole	No	8.05×10^{-7} M for Hypochlorite	Yes	No	Org. Biomol. Chem., 2022, 20, 4803–4814	hypochlorite and nerve agent mimic DCP
5.	Pyrene	Yes	0.04 ppm	Yes	No	Chem. Sci., 2022, 13, 2286–2295	hypochlorite
6.	Benzaldehyde–indole	No	1.18 nM for Hypochlorite	Yes	No	Analyst, 2021, 146, 5658–5667	cyanide and hypochlorite
7.	Phthalimide	No	6.4 ppb	Only N_2H_4	No	RSC Adv., 2021, 11, 21269–21278	N_2H_4
8.	diacetoxy-functionalized UiO-66 metal–organic framework	No	78.8 nM	Only N_2H_4	No	Dalton Trans., 2020, 49, 12565–12573	N_2H_4
9.	HydroxyBenzothiazolyl dihydroPyrazole	No	7.8 nM	Yes	No	New J. Chem., 2018, 42, 15990-	hypochlorite

						15996	
10.	Melamine-modified gold nanoparticle	No	0.1 µM for sulfite	No	No	Analyst, 2012, 137, 3437–3440	Sulfite and hypochlorite
11.	Coumarin	Yes	2 X 10^{-5} M^{-1}	No	No	Anal. Methods, 2013, 5, 2653	N_2H_4
12.	4-hydroxynaphthalimide-derived ratiometric fluorescent	Yes	2.1 × 10^{-8} M	Only N_2H_4	No	Sensors and Actuators B: Chemical, 2015, 208, 512-517	N_2H_4
13.	1,8-naphthalimide derivative	Yes	9.40 ± 0.12 nM	Only N_2H_4	No	Sens. Actuators, B, 2016, 227, 411–418	N_2H_4
14.	Isoniazid	No	No	No	No	Journal of Pharmaceutical and Biomedical Analysis, 2007, 43, 1213–1220	formation of equimolar quantities of hydrazine or ammonia during degradation of the drug to isonicotinic acid and isonicotinamide, respectively.
15.	Acetone azine or acetone azine-d12	No (in situ derivatization-headspace GC–MS)	limit of quantitation (LOQ) as low as 0.1 ppm when the API (active pharmaceutical ingredient) samples are prepared at 10 mg per headspace injection vial	No	No	Journal of Pharmaceutical and Biomedical Analysis, 2009, 49, 529–533	hydrazine in drug substances using in situ derivatization-headspace GC–MS
16.	Derivatization of hydrazine with ortho-phthalaldehyde (OPA) in water	No (method by GC–MS)	LOD and LOQ in this study were calculated as 0.002 and 0.007 g L^{-1}	No	No	Analytica Chimica Acta, 2013, 769, 79-83	Determination of hydrazine in water by gas chromatography –mass spectrometry
17.	Ortho-phthaldialdehyde Derivative	No	8.5 × 10^{-11} M	No	No	*Anal. Chem*., 2015, **87**,	Surface-Enhanced

						6460–6464	Raman Spectroscopy-Based Approach Detection of Hydrazine
18.	Fluorescein amide system	No	40 mM	Yes	No	*Chem. Commun., 2011, 47, 11978–11980*	OCl^-
19.	Acedan	No	16.6 nM	Yes	No	*J. Am. Chem. Soc. 2015, 137, 18, 5930–5938*	OCl^-
20.	benzo[d]thiazol-2-yl)-3-(8-methoxyquinolin-2-yl)acrylonitrile	Yes	hydrazine and OCl– 2.25×10^{-8} M and 3.46×10^{-8} M respectively	Yes	Yes	Present Work	Hypochlorite and Hydrazine

18. References:

[1] G. M. Sheldrick, *Acta Cryst.* 2008, **A64**, 112-122; (b) G. M. Sheldrick, *Acta Cryst.* 2015, **C71**, 3-8.

[2] A.D. Becke, J. Chem. Phys. 98 (1993) 5648–5652.

[3] C. Lee, W. Yang, R. G. Parr, Phys. Rev. B 37 (1988) 785–789.

[4] D. Andrae, U. Haeussermann, M. Dolg, H. Stoll and H. Preuss, Theor. Chim. Acta 77 (1990) 123–141.

[5] P. J. Hay, W. R. Wadt, J. Chem. Phys. 82 (1985) 299.

[6] R. Bauernschmitt, R. Ahlrichs, Chem. Phys. Lett. 256 (1996) 454–464.

[7] R.E. Stratmann, G.E. Scuseria, M.J. Frisch, J. Chem. Phys. 109 (1998) 8218–8224.

[8] M.E. Casida, C. Jamorski, K.C. Casida, D.R. Salahub, J. Chem. Phys. 108 (1998) 4439–4449.

[9] V. Barone, M. Cossi, J. Phys. Chem. A 102 (1998) 1995–2001.

[10] M. Cossi, V. Barone, J. Chem. Phys. 115 (2001) 4708–4717.

[11] M. Cossi, N. Rega, G. Scalmani, V. Barone, J. Comput. Chem. 24 (2003) 669–681.

[12] Gaussian 09, Revision D.01, M. J. Frisch, G. W. Trucks, H. B. Schlegel, G. E. Scuseria, M. A. Robb, J. R. Cheeseman, G. Scalmani, V. Barone, B. Mennucci, G. A. Petersson, H.

Nakatsuji, M. Caricato, X. Li, H. P. Hratchian, A. F. Izmaylov, J. Bloino, G. Zheng, J. L. Sonnenberg, M. Hada, M. Ehara, K. Toyota, R. Fukuda, J. Hasegawa, M. Ishida, T. Nakajima, Y. Honda, O. Kitao, H. Nakai, T. Vreven, J. A. Montgomery, Jr., J. E. Peralta, F. Ogliaro, M. Bearpark, J. J. Heyd, E. Brothers, K. N. Kudin, V. N. Staroverov, R. Kobayashi, J. Normand, K. Raghavachari, A. Rendell, J. C. Burant, S. S. Iyengar, J. Tomasi, M. Cossi, N. Rega, J. M. Millam, M. Klene, J. E. Knox, J. B. Cross, V. Bakken, C. Adamo, J. Jaramillo, R. Gomperts, R. E. Stratmann, O. Yazyev, A. J. Austin, R. Cammi, C. Pomelli, J. W. Ochterski, R. L. Martin, K. Morokuma, V. G. Zakrzewski, G. A. Voth, P. Salvador, J. J. Dannenberg, S. Dapprich, A. D. Daniels, Ö. Farkas, J. B. Foresman, J. V. Ortiz, J. Cioslowski, and D. J. Fox, Gaussian, Inc., Wallingford CT, 2009.